Hamida, Z. and Goulet, J-A. (Preprint 2020). *Network-Scale Deterioration Modelling of Bridges Based on Visual Inspections and Structural Attributes.* Structural Safety.

Network-Scale Deterioration Modelling of Bridges Based on Visual Inspections and Structural Attributes

Zachary Hamida*and James-A. Goulet
Department of Civil, Geologic and Mining Engineering
Polytechnique Montreal, CANADA

September 21, 2020

Abstract

Managing and maintaining bridges on a network-scale is directly associated with the capacity to monitor and forecast the deterioration state of these bridges. Data-driven models such as state-space models (SSM) has been effectively utilized for modelling the deterioration behaviour based on visual inspections of bridge network. However, such a model relies only on the inspection data and does not take into account the structural attributes of each bridge. In addition, the capacity for estimating the deterioration speed is limited, especially in cases with limited number of inspections. In this study, we combine the SSM deterioration model with a kernel regression (KR) method. The SSM-KR framework improves the estimates of the deterioration speed and reduces the overall bias in forecasting the deterioration. The role of KR is to model patterns between the deterioration speed and the structural attributes. Verification and validation of the SSM-KR model are done using synthetic data and real data respectively, whereby the real data is taken from a Canadian bridge network. In addition, the performance of SSM-KR is benchmarked against the existing SSM model using an independent test set of real inspections.

1 Introduction

Bridge management on a network-scale relies essentially on information about the deterioration state of bridges and their performance over time. There are different types of monitoring systems that provide such information about structures [1]. Out of these systems, visual inspections is the most widespread among infrastructure owners [23, 31, 22, 5]. Visual inspections are hands-on inspections performed on site by teams of inspectors. The upside of visual inspections is that it provides direct assessment that takes into account all the information available about the deterioration state of the structure [1]. The downside,

*Corresponding author: zachary.hamida@polymtl.ca

however, is that the inspections results have high variability over time due to the subjective nature of the evaluation [1, 27, 6]. The frequency of visual inspections can vary across bridges due to different factors, but it is commonly performed on a bi-annual basis [5]. This fact limits the amount of data available for modeling the deterioration behaviour, especially when considering that routine and/or major interventions can take place at any point in a time window of 5 to 15 years [14]. Different types of data-driven models have been proposed in the literature to model the deterioration behaviour while relying on visual inspection data [31, 35, 37]. *Discrete Markov models* (DMM) are largely utilized in modeling the deterioration based on visual inspections [31, 17, 18, 16, 8, 10, 33, 38]. In addition to the classical DMM, variations such as the *semi-Markov model* have been utilized to compensate for some of the drawbacks in DMM [26, 28, 37]. Several limitations are associated with the aforementioned Markov models which are briefly discussed in the work of Zambon et al. [36] and Hamida and Goulet [13]. Regression based-methods have been also utilized in performing analyses with visual inspections data [35, 15, 20]. However, the application of regression models is limited in comparison with the DMM models. This is mainly attributed to difficulties in modeling the temporal dependence from short time series, selecting attributes, and the offline training and validation processes [12, 13, 21, 9]. Nonetheless, from the small sample of regression-based studies, it is evident that some of the structural attributes can convey information about the structural deterioration pattern over time [15].

The main limitation common across all of the aforementioned deterioration modelling approaches is not taking into account the uncertainty associated with the inspectors [12, 13]. This has a major impact on the predictive capacity of the model, knowing that the amount of the inspection data is limited and the variability is high. Bayesian approaches such as *state-space models* (SSM) have successfully accommodated the inspectors' uncertainty within the deterioration model [13]. The SSM model relies on a kinematic model for describing the deterioration condition, speed and acceleration over time. One of the stated limitations associated with the SSM deterioration model is that the estimation of the deterioration speed is limited [13]. This limitation can impact the long-term forecast and in some case the short-term forecast if there are not enough inspection data. In addition, the SSM model relies on the inspection data only, and does not take into account the attributes of the structural elements (i.e. location or material). Structural attributes can be of high importance because they can be used to explain and learn some of structural deterioration patterns. For example, different regions may impose different external factors (e.g. cold vs. warm weather), which can affect the deterioration rate accordingly, not to mention also that each material has a unique aging process.

The aim of this study is to improve the short and long term forecast of the SSM deterioration model by taking advantage of the structural similarities across the network of bridges. This is done by deriving a hybrid framework that combines the SSM deterioration model with a kernel regression model for handling structural attributes. The proposed framework improves the estimate of the deterioration speed and reduces the overall bias in forecasting

the deterioration. The aforementioned improvements can provide a good prior estimate which compensates for the lack of inspection data in some of the structural elements. The new model performance is benchmarked against the SSM model using an independent test set of real inspections from a subset of bridges, in addition to being verified with synthetic data.

1.1 Nomenclature

The transportation network of bridges is defined by $\mathcal{B} = \{b_1, b_2, \ldots, b_{\mathtt{B}}\}$, which includes the information about each bridge b_j. These information include the structure's attributes $\boldsymbol{\mathcal{Z}} = \{\boldsymbol{z}_1, \boldsymbol{z}_2, \ldots, \boldsymbol{z}_{\mathtt{B}}\}$, where $\boldsymbol{z}_j$ is a vector representing the structural attributes of the j-th bridge. The attributes of interest in this study are: z_j^1 the structure's material, z_j^2 the age of the structure and z_j^3 the structure's location represented by the latitude. The structural elements associated with each bridge b_j are represented by the set $\mathcal{E}_j = \{e_1^j, e_2^j, \ldots, e_{\mathtt{E_j}}^j\}$. For each structural element e_p^j there is a chronological list of inspection data. The inspections information include the inspection time t, the engineer $I_i \in \mathcal{I} = \{I_1, I_2, \ldots, I_{\mathtt{I}}\}$ responsible for evaluating the p-th structural element e_p^j, and the condition of the structural element $\tilde{y} \in [l, u]$, with l representing the worst possible condition that can be assigned to a structural element and u representing the best condition. The symbol $(\sim)$ in $\tilde{y}$ is utilized to differentiate between observations in the bounded space $[l, u]$ and unbounded space $\mathbb{R}$.

2 Methodology

This section describes the proposed framework for factoring structural attributes in the deterioration analyses along with visual inspections.

2.1 Modelling Deterioration with State-Space Models

According to the method proposed by Hamida and Goulet [13], state-space model (SSM) is utilized for estimating the underlying deterioration process based on visual inspection data. The state-space representation of the deterioration process can be described by two models, namely the *transition model* and the *observation model*, each defined as in,

$$\overbrace{\boldsymbol{x}_t = \boldsymbol{A}\boldsymbol{x}_{t-1} + \boldsymbol{w}_t}^{\text{transition model}},\ \underbrace{\boldsymbol{w}_t : \boldsymbol{W} \sim \mathcal{N}(\boldsymbol{w}; \boldsymbol{0}, \boldsymbol{Q}_t)}_{\text{process errors}}, \tag{1}$$

$$\overbrace{y_t = \boldsymbol{C}\boldsymbol{x}_t + v_t}^{\text{observation model}},\ \underbrace{v_t : V \sim \mathcal{N}(v; 0, \sigma_V^2(I_i))}_{\text{observation errors}}. \tag{2}$$

The deterioration state at time t is defined by $\boldsymbol{x}_t : \boldsymbol{X} \sim \mathcal{N}(\boldsymbol{x}, \boldsymbol{\mu}_t, \boldsymbol{\Sigma}_t)$, $\boldsymbol{A}$ is the state transition matrix, $\boldsymbol{w}_t$ is the process error with $\boldsymbol{Q}_t$ representing the error covariance matrix. The transition model utilized is a discretized time-continuous kinematic model [3] which describes the condition x_t, the speed $\dot{x}_t$ and acceleration $\ddot{x}_t$. In Equation 2, y_t represents the observation, $\boldsymbol{C}$ is the observation matrix and $v_t : V \sim \mathcal{N}(v; 0, \sigma_V^2(I_i))$ is the observation error with $\sigma_V(I_i)$ being the standard deviation of the error associated with each inspector $I_i \in \mathcal{I}$ performing the inspections. In this study, the estimation of the hidden states is done using the *Kalman filter* (KF) [19] expressed in the short form as,

$$(\boldsymbol{\mu}_{t|t}, \boldsymbol{\Sigma}_{t|t}, \mathcal{L}_t) = \text{Kalman filter}(\boldsymbol{\mu}_{t-1|t-1}, \boldsymbol{\Sigma}_{t-1|t-1}, \boldsymbol{y}_t, \boldsymbol{A}_t, \boldsymbol{Q}_t, \boldsymbol{C}_t, \boldsymbol{R}_t), \tag{3}$$

where $\boldsymbol{\mu}_{t|t} \equiv \mathbb{E}[\boldsymbol{X}_t|y_{1:t}]$ is the posterior expected value and $\boldsymbol{\Sigma}_{t|t} \equiv \text{cov}[\boldsymbol{X}_t|y_{1:t}]$ is the posterior covariance at time t, given observations $\boldsymbol{y}_{1:t}$. The log-likelihood for each observation in $\boldsymbol{y}_t$ is represented by $\mathcal{L}_t$. In addition to the KF, the *Kalman smoother* (KS) [29] is utilized to improve the KF estimates retrospectively based on information from the entire time series. Appendix 3 provides details about the equations of KF and KS.

The health condition of a structural element, when no interventions are applied, has two characteristics: 1. monotonically decreasing, 2. changes are occurring within a predefined range of values. In order to accommodate the aforementioned properties, modifications are applied on the inspection data and the state-space model [13]. These modifications include performing space transformation on the inspection data using a *transformation function*. Performing space transformation allows the model's predictions and forecasts to be restricted within the range of feasible values, in addition, it allows the uncertainty to be state-dependent. The second modification is to impose monotonicity by ensuring the speed estimates are always in the negative domain. This is done by using the PDF truncation method proposed by Simon and Simon [30].

2.2 Kernel Regression (KR)

Kernel methods are well-known and frequently used for pattern detection and discrimination problems [4]. Kernel regression relies on a kernel function that provides information about the similarity between pairs of covariates. In this context, the purpose of employing KR is to incorporate information from the structural attributes $\boldsymbol{z}$ in the deterioration analysis of structural elements. KR is utilized to estimate the initial deterioration speed $\dot{x}_{0,p}^j$ associated with each structural element e_p^j. This estimation is based on the *Nadaraya-Watson* model [25] described by,

$$\dot{x}_{0,p}^j = (\boldsymbol{a}_p^j)^\intercal \dot{\boldsymbol{x}}_{\boldsymbol{z}} + w_0 : W_0 \sim \mathcal{N}(w_0; 0, \sigma_{w_0}^2), \tag{4}$$

with the vector $\boldsymbol{a}_p^j$ obtained by,

$$\boldsymbol{a}_p^j = \frac{\boldsymbol{k}\left(\boldsymbol{z}_j, \boldsymbol{Z}_{c(m)}, \boldsymbol{\ell}\right)}{\sum_{m=1}^{\mathtt{M}} \boldsymbol{k}\left(\boldsymbol{z}_j, \boldsymbol{Z}_{c(m)}, \boldsymbol{\ell}\right)},\ m = 1, \ldots, \mathtt{M}, \tag{5}$$

where $\boldsymbol{z}_j$ is a vector of $\mathtt{Q}$ covariates associated with the j-th bridge and $\boldsymbol{Z}_c$ is a matrix that encodes a $\mathtt{Q}$-dimensional grid of reference points. The $\mathtt{Q}$-dimensional grid is obtained from discretizing the range of each covariate with an equal number of $\mathtt{M}$ reference points, such that $\boldsymbol{Z}_c = \left[\boldsymbol{z}_c^1 \ \ldots \ \boldsymbol{z}_c^{\mathtt{Q}}\right] \in \mathbb{R}^{\mathtt{M}^{\mathtt{Q}} \times \mathtt{Q}}$. The function $\boldsymbol{k}(.)$ is a multivariate kernel function $\boldsymbol{k} : \mathbb{R}^{\mathtt{Q}} \rightarrow \mathbb{R}$ representing the multiplicative kernel,

$$\boldsymbol{k}\left(\boldsymbol{z}_j, \boldsymbol{Z}_{c(m)}, \boldsymbol{\ell}\right) = k\left(\frac{z_j^1 - \boldsymbol{z}_{c(m)}^1}{\ell_1}\right) \cdot \ldots \cdot k\left(\frac{z_j^{\mathtt{Q}} - \boldsymbol{z}_{c(m)}^{\mathtt{Q}}}{\ell_{\mathtt{Q}}}\right), \ m = 1, \ldots, \mathtt{M}. \tag{6}$$

where $k(.)$ is the univariate kernel function and $\boldsymbol{\ell} = [\ell_1 \ldots \ell_{\mathtt{Q}}]$ represents the bandwidth parameter associated with each covariate. Estimating the $\boldsymbol{\ell}$ parameters as well as the noise parameter σ_{w_0} is done using the parameter estimation framework described in Section 2.4. An example shown in Figure 1, illustrates the relation between the reference points $\boldsymbol{Z}_c$, the covariates $\boldsymbol{z}_j \in \boldsymbol{\mathcal{Z}}$, and the true response $\dot{x}_0$. In this graph, the true relation between the covariates z_1, z_2 and the response $\dot{x}_0$ is illustrated by the surface on top, while the reference points are represented by a 2D grid, which is defined by $\boldsymbol{z}_c^1$, $\boldsymbol{z}_c^2$ and the state $\dot{\boldsymbol{x}}_z$ represented by the expected value $\dot{\mu}_z$.

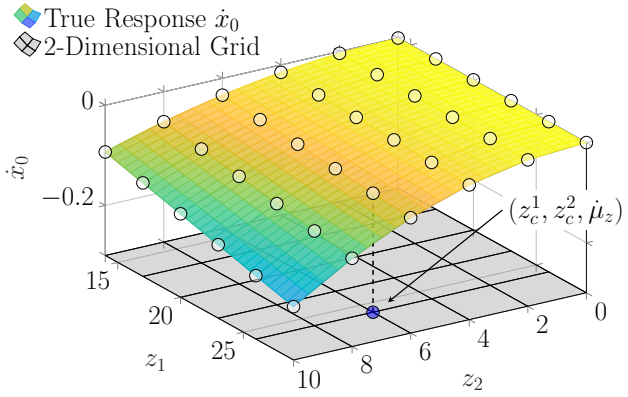

Figure 1: Example of the relation between covariates z_1, z_2 and true response $\dot{x}_0$, along with 2D grid defined by $\mathtt{M}^{\mathtt{Q}} = 6^2$ reference points with coordinates of z_c^1, z_c^2 and $\dot{x}_z$ represented by the expected value $\dot{\mu}_z$.

Estimating the hidden states $\dot{\boldsymbol{x}}_{\boldsymbol{z}}$, such that each $\dot{x}_z$ matches or approaches the true response $\dot{x}_0$ associated with (z_c^1, z_c^2), is done using the recursive framework detailed in Section 2.4.1.

2.3 Hybrid Deterioration Model SSM-KR

The full framework for estimating the deterioration state $\boldsymbol{x}_{t,p}^j$ over time is illustrated in Figure 2. For any structural element e_p^j in bridge $b_j \in \mathcal{B}$, the inspection data $\tilde{\boldsymbol{y}}_{t,p}^j$ and the structural attributes $\boldsymbol{z}_j$ are considered in the analyses. The structural attributes $\boldsymbol{z}_j$ are

utilized in the KR model to obtain an initial estimate for the deterioration speed $\dot{x}^j_{0,p}$, while the inspection data are transformed from the bounded space $\tilde{\boldsymbol{y}}^j_{t,p} \in [l, u]$ to the unbounded space $\boldsymbol{y}^j_{t,p} \in \mathbb{R}$ using the transformation function detailed in [13]. Furthermore, the expected initial deterioration condition is considered as $\mu^j_{0,p} = y^j_{1,p}$ with the variance ${\sigma^j_{0,p}}^2 = \sigma^2_0$ and the expected initial acceleration is $\ddot{\mu}^j_{0,p} = 0$ with the variance ${\ddot{\sigma}^j_{0,p}}^2 = \ddot{\sigma}^2_0$. Following the initialization step, the Kalman filter is utilized for propagating the initial state $\boldsymbol{x}^j_{0,p}$ forward in time through the prediction step and the update step up to time T. Similarly, the Kalman smoother is applied to refine the KF estimates from $t = T - 1$ to $t = 0$. At each time step t in KF and KS, the state estimate is examined with the following constraint $\dot{\mu}^j_{t,p} + 2\dot{\sigma}^j_{t,p} \leq 0$. The aforementioned constraint ensures the state estimate does not allow the structural element health to improve over time. If the constraint is violated, the PDF truncation method is applied [13, 30]. The outcome of the SSM-KR framework is denoted

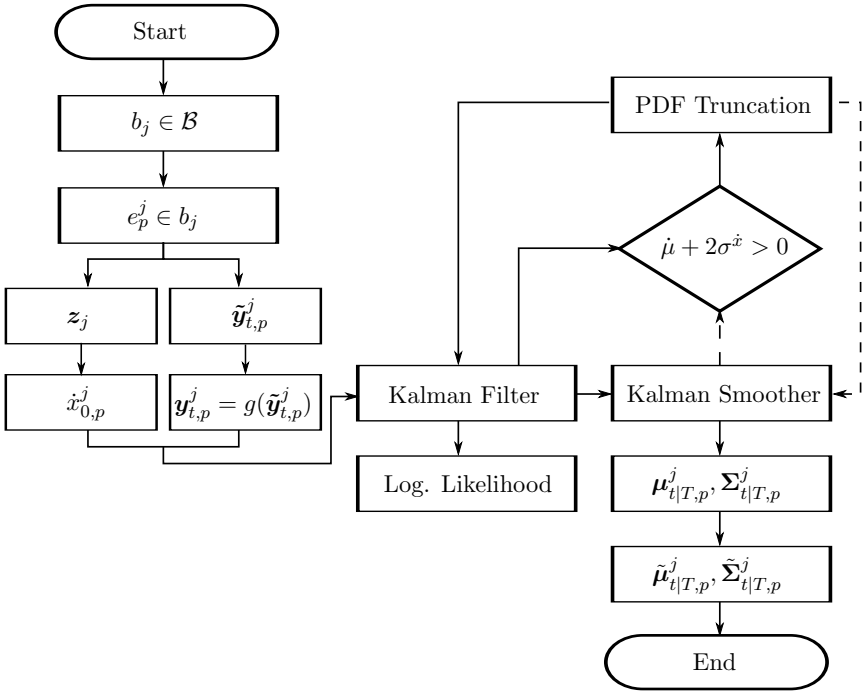

Figure 2: SSM-KR framework for estimating the deterioration state of structural element e^j_p from time t to time T.

by $\tilde{\boldsymbol{\mu}}^j_{t|T,p} \in [l, u]$ which represents the smoothed expected values for the deterioration state and $\tilde{\boldsymbol{\Sigma}}^j_{t|T,p}$ representing the smoothed variances at each time step t.

2.4 Model Parameters & Estimation Framework

In addition to the SSM model parameters [13], the SSM-KR model parameters include the kernel bandwidth parameters $\boldsymbol{\ell}$ and the kernel process error σ_{w_0}. The SSM-KR model parameters are grouped in the set,

$$\boldsymbol{\theta} = \left\{ \underbrace{\boldsymbol{\sigma_V}(I_{1:\mathtt{I}})}_{\text{Inspectors Std.}}, \overbrace{\sigma_W}^{\text{Process error}}, \underbrace{n}_{\text{Transform.}}, \overbrace{\sigma_0, \ddot{\sigma}_0, p_1, p_2}^{\text{Initial state}}, \underbrace{\sigma_{w_0}}_{\text{KR process error}}, \overbrace{\boldsymbol{\ell}}^{\text{Kernel bandwidth}} \right\}, \tag{7}$$

where $\boldsymbol{\sigma_V}(I_{1:\mathtt{I}})$ refers to the standard deviations associated with each inspector $I_i \in \mathcal{I}$, σ_w is the kinematic model process noise, n is the transformation function parameter and $\{\sigma_0, \ddot{\sigma}_0, p_1, p_2\}$ are the parameters related to the covariance of the initial state $\boldsymbol{\Sigma}^j_{0,p} = \text{diag}\left[\sigma_0^2\ \dot{\sigma}_0^2\ \ddot{\sigma}_0^2\right]$ with $\dot{\sigma}_0^2$ being defined by the following linear function,

$$\dot{\sigma}_0^2 = p_1^2(u - \tilde{\mu}_1) + p_2^2, \tag{8}$$

whereby $\tilde{\mu}_1$ is the expected value of the condition at $t = 1$, which is initially considered $\tilde{\mu}_1 = \tilde{y}_1$, and is updated later with the smoothed expected value as $\tilde{\mu}_1 = \tilde{\mu}_{1|T}$ [13]. All model parameters in Equation 7 are estimated using a *Maximum Likelihood Estimate* (MLE) which is defined by the network-scale log-likelihood as,

$$\mathcal{L}(\boldsymbol{\theta}) = \sum_{j=1}^{\mathtt{B}} \sum_{p=1}^{\mathtt{E}_j} \sum_{t=1}^{\mathtt{T}_p} \ln f(y^j_{t,p} | y^j_{1:t-1,p}, \boldsymbol{\theta}), \tag{9}$$

The parameters estimation procedure can be formulated as an optimization problem with the following constraints,

$$\begin{aligned} \boldsymbol{\theta}^* = \arg\max_{\boldsymbol{\theta}} \quad & \mathcal{L}(\boldsymbol{\theta}), \\ \text{subject to:} \quad & \sigma_w, \sigma_{w_0}, \sigma_0, \ddot{\sigma}_0, p_1, p_2, \ell > 0, \\ & \sigma_V(I_i) > 0,\ \forall I_i \in \mathcal{I}, \\ & n \in \{1, 2, 3, 4, 5\}. \end{aligned} \tag{10}$$

The optimization problem above is solved by using a gradient-based optimization framework for all parameters $\boldsymbol{\theta}$ which is detailed in Section 2.4.2. In order to ensure that the deterioration model is not overfitting, the database is split into a training, validation, and testing set. The split of the data is done randomly and bridge-wise such that the structural elements of one bridge can not exist in the training set and the validation/testing set at the same time.

2.4.1 Recursive Estimation for the Deterioration Speed

The estimation of the hidden states $\dot{\boldsymbol{x}}_{\boldsymbol{z}}$ is done recursively by relying on the Kalman smoother estimates. At the beginning, $\dot{\boldsymbol{x}}_{\boldsymbol{z}}$ is initialized with an expected value $\dot{\boldsymbol{\mu}}_{\boldsymbol{z}=\mathbf{0}}$ and a variance $\dot{\boldsymbol{\Sigma}}_{\boldsymbol{z}} = \text{diag}(\mathbf{4})$ so that it represents a weakly informative prior. Estimating $\dot{\boldsymbol{x}}_{\boldsymbol{z}}$ is done based on the structural elements in the training set as in,

$$\begin{aligned} \boldsymbol{J}_z &= \dot{\boldsymbol{\Sigma}}_{\boldsymbol{z}} \boldsymbol{A}_{\kappa}^{\intercal} \dot{\boldsymbol{\Sigma}}_{0|\boldsymbol{z}}^{-1}, \\ \dot{\boldsymbol{\mu}}_{\boldsymbol{z}|T} &= \dot{\boldsymbol{\mu}}_{\boldsymbol{z}} + \boldsymbol{J}_z(\dot{\boldsymbol{\mu}}_{0|T} - \dot{\boldsymbol{\mu}}_{0|\boldsymbol{z}}), \\ \dot{\boldsymbol{\Sigma}}_{\boldsymbol{z}|T} &= \dot{\boldsymbol{\Sigma}}_{\boldsymbol{z}} + \boldsymbol{J}_z(\dot{\boldsymbol{\Sigma}}_{0|T} - \dot{\boldsymbol{\Sigma}}_{0|\boldsymbol{z}})\boldsymbol{J}_z^{\intercal}, \end{aligned} \tag{11}$$

where $\boldsymbol{A}_{\kappa}$ is an array of vectors $\boldsymbol{a}_p^j$ as in $\boldsymbol{A}_{\kappa} = \left[\boldsymbol{a}_1^1 \cdots \boldsymbol{a}_p^j\right]^{\intercal}$, $\dot{\boldsymbol{\mu}}_{0|\boldsymbol{z}}$ and $\dot{\boldsymbol{\Sigma}}_{0|\boldsymbol{z}}$ are the expected value and the covariance matrix for the speed at time $t = 0$, as predicted by Equation 4, for all structural elements. The expected value vector $\dot{\boldsymbol{\mu}}_{0|T}$ and the covariance matrix $\dot{\boldsymbol{\Sigma}}_{0|T}$ represent the SSM smoothed estimates for the deterioration speed at time $t = 0$ and for all structural elements. At the beginning, the SSM estimation of the deterioration speed is based on the initial values $\dot{\mu}_{0,p}^j = 0$ and $\dot{\sigma}_{0,p}^j{}^2 = \dot{\sigma}_0^2$. After each update of $\dot{\boldsymbol{x}}_{\boldsymbol{z}}$, the expected value $\dot{\mu}_{0,p}^j$ of the SSM is updated by Equation 4 with $\dot{\mu}_{0,p}^j = \dot{\mu}_{0,p|\boldsymbol{z}}^j$, while the KR variance is reinitialized with $\boldsymbol{\Sigma}_{\boldsymbol{z}} = \text{diag}(\mathbf{4})$. The SSM variance $\dot{\sigma}_{0,p}^j{}^2$ is not updated because the KR model has a large variance initially which affects the SSM model performance negatively. The update processes in Equation 11 and in the SSM prior are repeated recursively until the MLE estimate of the validation set is no longer improving. Thereafter, the KR model is utilized in providing the full prior estimate of the speed $\dot{x}_{0,p}^j$ for any structural element e_p^j.

2.4.2 Parameters & Hidden State Estimation Framework

The gradient algorithm employed in this framework is the *Newton-Raphson* algorithm [11]. The estimation framework starts with optimizing the initial set of parameters $\boldsymbol{\theta}^s = \{\sigma_w, \sigma_V, \sigma_0^x, \sigma_0^{\dot{x}}, p_1, p_2\}$, where σ_V is the observation uncertainty parameter common for all inspectors $\boldsymbol{\sigma_V}(I_{1:\mathtt{I}}) = \sigma_V$. Following this step, the optimization framework updates the inspectors parameters by iteratively optimizing each parameter $\sigma_V(I_i)$, while keeping the rest of model parameters $\boldsymbol{\theta}$ fixed. The convergence for $\sigma_V(I_i)$ parameters is determined by either having the difference in $\mathcal{L}$ (validation set) less than the tolerance ϵ, or if the stall limit is reached. The stall is the number of iterations with no significant improvements in the objective function. Upon the convergence of $\sigma_V(I_i)$, the model parameters in $\boldsymbol{\theta}^m = \{\sigma_w, \sigma_0^x, \sigma_0^{\dot{x}}, p_1, p_2\} \subset \boldsymbol{\theta}$ are updated by the optimization algorithm. Thereafter, the recursive estimation for $\dot{\boldsymbol{x}}_{\boldsymbol{z}}$ is carried out using the framework presented in Section 2.4.1. The initial estimation of $\dot{\boldsymbol{x}}_{\boldsymbol{z}}$ is done based on the initial KR model parameters $\boldsymbol{\theta}^{\kappa} = \{\sigma_{w_0}, \boldsymbol{\ell}\} \subset \boldsymbol{\theta}$. Following the optimization of $\boldsymbol{\theta}^{\kappa}$, the state $\dot{\boldsymbol{x}}_{\boldsymbol{z}}$ is refined in accordance with the new KR parameters. The estimation procedure for the inspectors' parameters, the parameters in $\{\boldsymbol{\theta}^m, \boldsymbol{\theta}^{\kappa}\}$ and the state $\dot{\boldsymbol{x}}_{\boldsymbol{z}}$ is repeated recursively until the global convergence

criteria is met. Finally, the parameter $n \in \{1, 2, 3, 4, 5\}$ is identified by repeating the full optimization procedure for each value of n [13]. The pseudo code which illustrate the details of the aforementioned framework is shown Appendix 1.

3 Case Studies

This section presents the case studies that are considered in demonstrating the SSM-KR model performance.

3.1 Visual Inspection Data

The database for the real inspection data is taken from the network of $\mathtt{B} \approx 10000$ bridges located in the province of Quebec, Canada. The deterioration state of any structural element e_p^j is represented by 4 damage severity categories [22]. Those categories are: A: *Nothing to little*, B: *Medium*, C: *Important* and D: *Very Important*. The inspector have to assign the percentage of the structural element area under each category, such that $0\% \leq y_a, y_b, y_c, y_d \leq 100\%$ and the sum $y_a + y_b + y_c + y_d = 100\%$. For example, $y_a = 80\%,\ y_b = 10\%,\ y_c = 10\%,\ y_d = 0\%$ refers to 80% of the structural element area has no damage, 10% has medium damage, 10% has important damage and no very important damages. The aforementioned representation of the deterioration state can be aggregated into a single metric [13] as in,

$$\tilde{y} = \omega_1 y_a + \omega_2 y_b + \omega_3 y_c + \omega_4 y_d, \tag{12}$$

with $\omega_{1:4}$ represent the utilities defined as: $\omega_1 = 100$, $\omega_2 = 75$, $\omega_3 = 50$, $\omega_4 = 25$, and $\tilde{y}$ represents the aggregated observation [13]. Hence, the deterioration condition of any structural element is a continuous numerical value within the range $\tilde{y} \in [25, 100]$. For example, a prefect state $(y_a = 100\%, y_b = 0\%, y_c = 0\%, y_d = 0\%)$ is equivalent to $\tilde{y} = 100$ and a very damaged state $(y_a = 0\%, y_b = 0\%, y_c = 0\%, y_d = 100\%)$ is equivalent to $\tilde{y} = 25$.

3.2 Synthetic Visual Inspection Data

The main advantage of performing analyses with synthetic data is that the true deterioration state is known, which allows verifying the deterioration model performance. The generated synthetic dataset resembles quantitatively and qualitatively the real database of visual inspections. The true deterioration state for each structural element is generated based on the transition model in Equation 1, while the observations are generated based on the observation model in Equation 2. The standard deviation associated with each inspector I_i is generated based on a Uniform distribution as in $\sigma_V(I_i) \sim \mathcal{U}(1, 6)$, and the standard deviation for the process error of the kinematic model is $\sigma_w = 5 \times 10^{-3}$. The rest of the qualitative characteristics of the deterioration process, such as the deterioration condition

and speed thresholds, are adopted from the criteria defined in Hamida and Goulet [13]. Quantitatively, the deterioration of each synthetic structural element is represented by a continuous numerical value with $\tilde{y} \in [25, 100]$. The number of inspections per element varies from 3 to 5 inspections for the majority of elements with few elements having 6 to 8 inspections. The average service life of the synthetic structural element is assumed to be 60 years. In order to generate a structural attribute for the synthetic dataset, it is assumed that the true deterioration speed exhibit the following relation with z_j,

$$z_j = \log(|\dot{x}_0^j|) + w_0 : W_0 \sim \mathcal{N}(w_0; 0, 0.1^2), \tag{13}$$

Generating the synthetic attribute z_j allows verifying the performance of the recursive estimation framework presented in Section 2.4.1.

4 Deterioration Analyses with SSM-KR

This section presents the analyses performed using the SSM-KR framework on synthetic and real inspection datasets.

4.1 Model Verification Using Synthetic Data

The synthetic training dataset consists of $\mathtt{E} = 16500$ structural elements with a total of $\mathtt{I} = 223$ inspectors providing the observations in each time-series. The synthetic structural attribute z_j associated with each structural element is illustrated in the histogram shown in Figure 3, where it can be noticed that the distribution of $\boldsymbol{z}$ values has a long tail with the

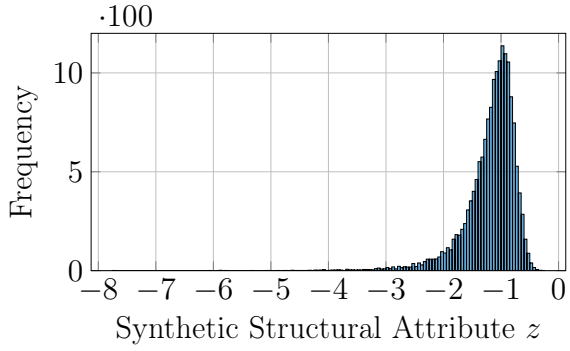

Figure 3: Histogram of synthetic structural attribute z.

majority of the values concentrated within the range $[-2, -0.5]$. Factoring the information from the structural attribute z in the deterioration analyses is done through the KR model. The kernel function utilized in this case is the *radial basis function* (RBF) [7]. The total number of reference points $\boldsymbol{z}_c$ is $\mathtt{M} = 20$, which is also equivalent to the total number of

hidden states in $\dot{\boldsymbol{x}}_{\boldsymbol{z}}$. The estimation for $\dot{\boldsymbol{x}}_{\boldsymbol{z}}$ in Equation 4 is done based on the recursive framework presented in Section 2.4.1. Figure 4 illustrates the initial expected value $\dot{\boldsymbol{\mu}}_{\boldsymbol{z}}$ and the updated state $\dot{\boldsymbol{x}}_{\boldsymbol{z}}$ following convergence after 3 iterations in the recursive framework. In Figure 4, it can be noticed that the $\dot{\boldsymbol{x}}_{\boldsymbol{z}}$ estimates are deviating from the true curve when $z < -2$. This is because the range of values $\boldsymbol{z} \in [-8, -2]$ is associated with the tail of the distribution (Figure 3), where few or no data is available. An example for the effect

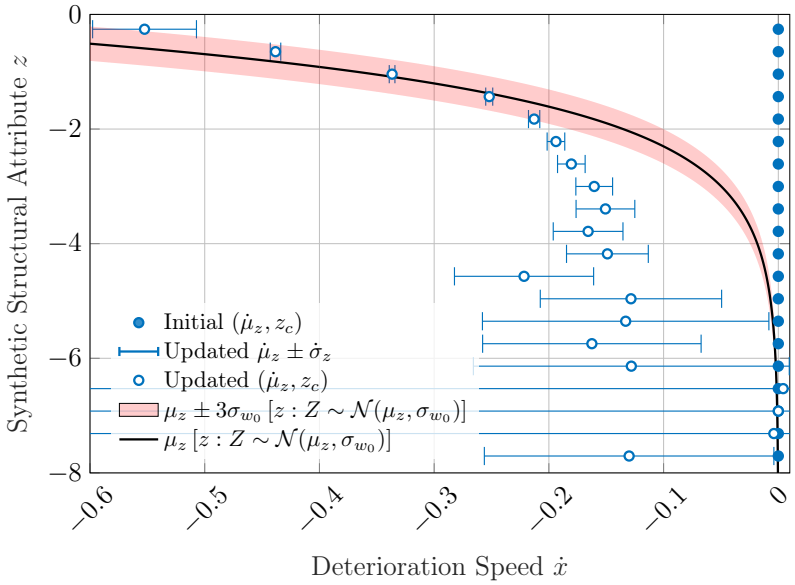

Figure 4: Comparison between the updated estimates $\dot{\mu}_z$ (iteration #3) at each reference point $z_c \in \boldsymbol{z}$ and the true relation between the synthetic structural attribute z and the deterioration speed $\dot{x}_z$.

of the state $\dot{\boldsymbol{x}}_{\boldsymbol{z}}$ convergence on the KR model performance is presented in Figure 5. In this example, it is shown that after each $\dot{\boldsymbol{x}}_{\boldsymbol{z}}$ update, the expected value from KR $\dot{\mu}^j_{0,p}$ is approching the true speed $\dot{x}^j_{0,p}$.

In order to assess the network-scale improvement in estimating the initial deterioration speed, a comparison between the error histogram of the SSM-KR model and the SSM model is shown in Figure 6. The errors are determined by the difference between the true initial speed and the smoothed estimate of the initial speed from each model. From the two histograms in Figure 6, it is noticed that the new formulation reduces the bias in the initial speed estimate. The parameter estimation for the SSM-KR model is done using the gradient-based optimization framework detailed in Section 2.4.2. The estimated model parameters are shown in Figure 7 for the inspectors parameters and Table 1 for the rest of model parameters. In Figure 7, the alignment of the scatter with the diagonal verifies the capacity of the optimization framework in estimating the inspectors' parameters, where the

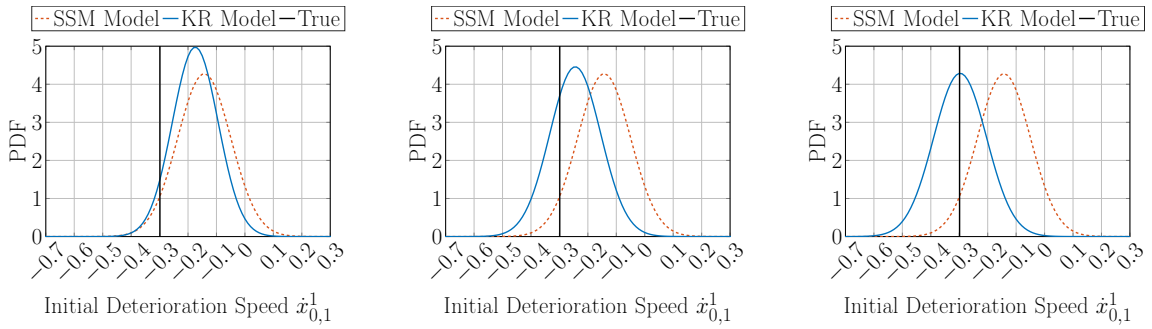

(a) Iteration #1 SSM-KR. (b) Iteration #2 SSM-KR. (c) Iteration #3 SSM-KR.

Figure 5: Recursive estimation of the state $\dot{x}^j_{0,p}$ illustrated by the probability density function (PDF) with the true speed represented by the vertical line and the SSM model represented by a dashed line.

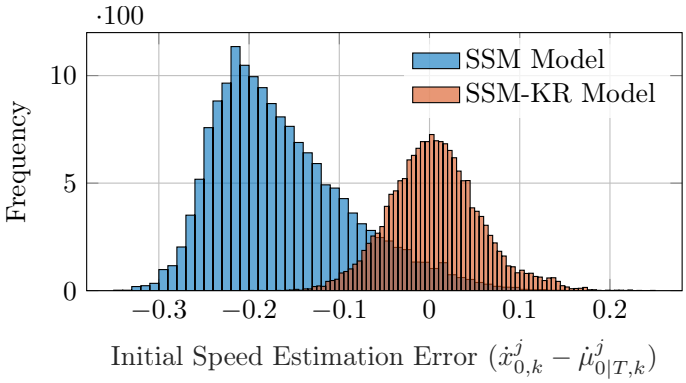

Figure 6: Comparison between the SSM-KR model errors histogram (right) and the SSM model errors histogram (left), with the errors determined by the difference between the true initial speed and the smoothed estimate of the initial speed.

Table 1: Estimation results of model parameters for synthetic data.

σ_w	σ_0^x	σ_V	$\sigma_0^{\ddot{x}}$	p_1	p_2	n	σ_{w_0}	$\ell^{\texttt{RBF}}$
3.787×10^{-3}	1.001	3.001	0.0498	0.0499	0.1488	4	0.1238	0.1933

dashed line represents the initial estimate σ_V for all the inspectors' parameters $\sigma_V(I_i)$. Example of time-series analyses using the SSM-KR model is shown in Figures 8 and 9. In this example, both SSM-KR and SSM (without factoring the structural attribute) are utilized in producing the deterioration estimates of the condition and the speed. From

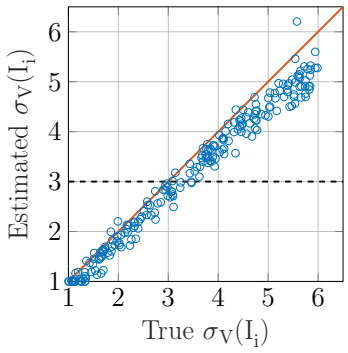

Figure 7: Estimation results for synthetic inspectors parameters $\sigma_V(I_i)$ (total: 223 inspectors) with dashed line referring to the initial estimate for all $\sigma_V(I_i)$ parameters.

Figure 8, the condition estimates of SSM-KR and SSM are overlapping initially, however, these estimates starts to diverge over time due to the difference in the initial speed estimate of each model. It can be noticed in this example that the true state represented by a dashed line is within the confidence interval of the SSM-KR model. The speed estimate

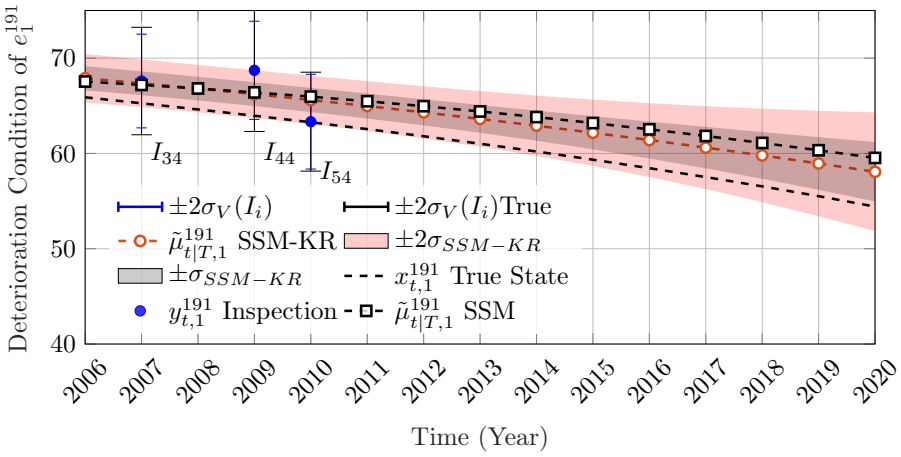

Figure 8: Deterioration condition estimate for synthetic structural element e_1^{191}, with the *circle* marker representing the SSM-KR estimates, the *square* marker representing SSM estimates and the true condition represented by a dashed line.

associated with the aforementioned example is shown in Figure 9. It can be noticed that the overall estimate for the speed in the SSM-KR model is better than SSM given the true deterioration speed.

In order to examine the network-scale improvements, Figure 10 illustrates the average error in forecast time for the condition and the speed based on the SSM-KR model and

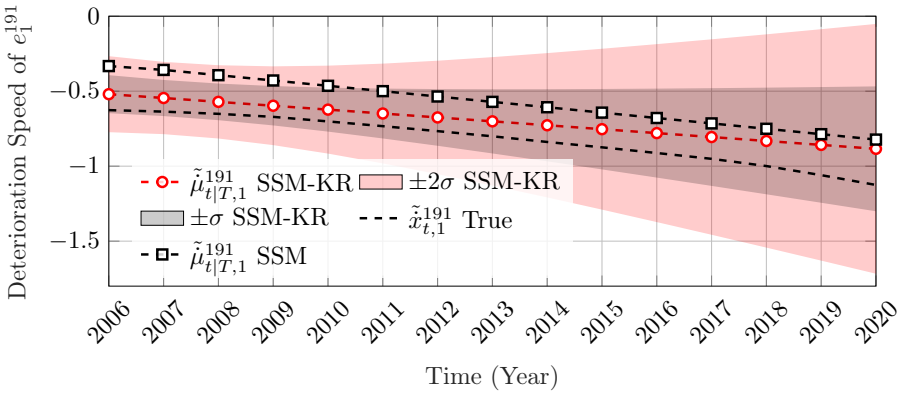

Figure 9: Deterioration speed of synthetic structural element e_1^{191}, with the *circle* marker representing the SSM-KR estimates, the *square* marker representing SSM estimates and the true state represented by a dashed line.

the SSM model. From Figure 10a, it can be noticed that the average error in SSM-KR

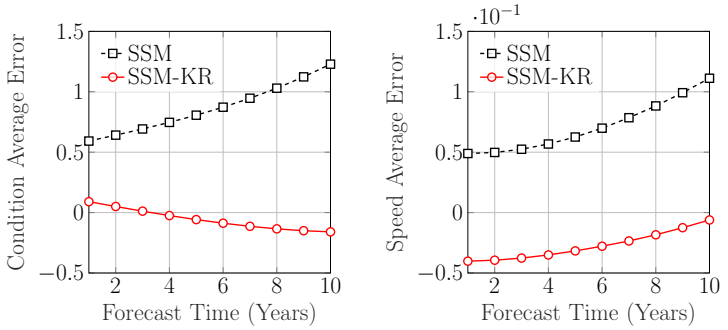

(a) Average error in the condition estimate.

(b) Average error in the speed estimate.

Figure 10: Average error comparison between SSM-KR & SSM estimates for the condition and speed in synthetic data.

condition estimate is near zero throughout the time-window of analyses, while the average error in SSM is diverging monotonically away from zero. From this, it can be concluded that factoring information about the structural attribute has reduced the overall bias in estimating the deterioration condition. On the other hand, in Figure 10b, the speed estimates in both models are changing monotonically with the SSM model speed estimates diverging similarly to the SSM condition estimates.

4.2 Model Validation with Real Data

The validation analyses are performed on the structural element category *Beam*. A structural element is considered in the deterioration analyses if it has 3 or more inspections without interventions [13]. The total number of beam elements that are considered in the deterioration analyses is: $\mathtt{E} = 16689$ elements taken from $\mathtt{B} = 2133$ bridges. The number of inspectors involved in this dataset is $\mathtt{I} = 223$. The inspections dataset is divided into a training set with $\mathtt{E_{tr}} = 13639$ structural elements from $\mathtt{B_{tr}} = 1915$ bridges, validation set with $\mathtt{E_v} = 2034$ structural elements from $\mathtt{B_v} = 142$ bridges and a testing set having $\mathtt{E_t} = 1016$ structural elements from $\mathtt{B_t} = 76$ bridges.
The structural attributes $\boldsymbol{z}_j$ considered in the analyses are: z_j^1 the structure's material, z_j^2 the age of the structure and z_j^3 the structure's location represented by the latitude. In order to determine the relevance of each attribute to the response, the preliminary analysis involved a larger number of structural attributes. The selection of attributes is based on the kernel bandwidth parameters in $\boldsymbol{\ell}$, which are estimated based on the inspection data and using the MLE approach [24, 34]. If an estimated kernel bandwidth ℓ converges to a large value relative to the range of the covariate, then the inverse of ℓ will result in the covariate z being almost independent of the response [34]. The histogram for each of the selected attributes is shown in Figure 11. It should be noted that the age of the bridge is determined

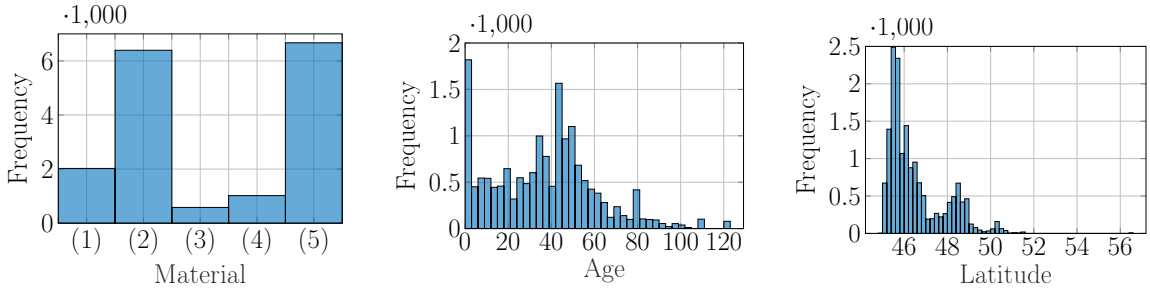

(a) Histogram of material, (1): weatherproof steel, (2): steel, (3): wood, (4): concrete (HP), (5): concrete.

(b) Histogram of structures age calculated at the date of the first inspection point.

(c) Histogram of latitude (bridge location).

Figure 11: Frequency of each structural attribute from real data

by deducting the date of the first inspection point from the construction date of the bridge. The multivariate KR analyses involves different types of kernel functions. The selection of the kernel function is done based on the type of data (i.e. categorical or continuous) and the MLE estimate. In this case study, the structure's material is assumed to be unordered categorical data, which can be modelled using the Aitchison and Aitken [2] (AAK) kernel function. The kernel bandwidth in the AAK function is bounded by $0 \leq \ell \leq \frac{\mathtt{C}-1}{\mathtt{C}}$, where $\mathtt{C}$ is the number of categories [32]. The structure's age and latitude are analyzed using the

Matérn 12 (M12) kernel function. In addition to the structural attributes, the condition of the structural element at the first inspection point is also included as a covariate in the multivariate KR. The kernel function utilized for the condition is the *Matérn 52* (M52). The equations for each of the aforementioned kernel functions are available in Appendix 2. The estimated SSM-KR model parameters are shown in Table 2, while the inspectors parameters are shown in Figure 12.

Table 2: Estimation results of SSM-KR parameters for real data.

σ_w	σ_0^x	σ_V	$\sigma_0^{\ddot{x}}$	p_1	p_2	n
5.451×10^{-3}	1.025	2.220	0.0499	0.1238	0.1933	4
σ_{w_0}	$\ell^{\texttt{AAK}}$	$\ell^{\texttt{M12}}$	$\ell^{\texttt{M12}}$	$\ell^{\texttt{M52}}$		
0.1292	0.0166	12.6064	1.4309	7.2166		

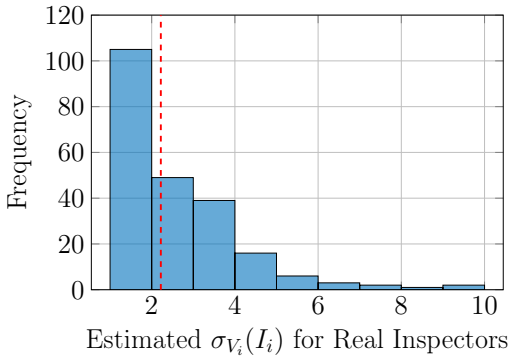

Figure 12: Histogram for the estimated parameters $\sigma_V(I_i)$ of real inspectors (total: 223 inspectors) with the dashed line referring to the initial estimate for all $\sigma_V(I_i)$.

In order to demonstrate the performance of SSM-KR in the real case, two examples are considered from the test set. The first example is for the structural element e_{10}^{244} from bridge b_{244}. This bridge was $z_{244}^2 = 61$ years of age at the time of the first inspection, it is located at a latitude $z_{244}^3 \approx 48$, and the material of the beam elements is $z_{244}^1 =$ steel.
The deterioration analyses for the structural element e_{10}^{244} from b_{244} are shown in Figures 13 and 14. Figure 13 illustrates a comparison between the condition estimates of SSM-KR represented by the *circle* marker and the SSM represented by the *square* marker. It can be noticed that SSM-KR estimates adapt in a better way to the recorded observation compared to the SSM estimates. Furthermore, the same comparison is performed for the deterioration speed estimates from each model. From Figure 14, throughout the prediction time, the speed estimates of SSM-KR shows a consistent progression in comparison to the SSM speed

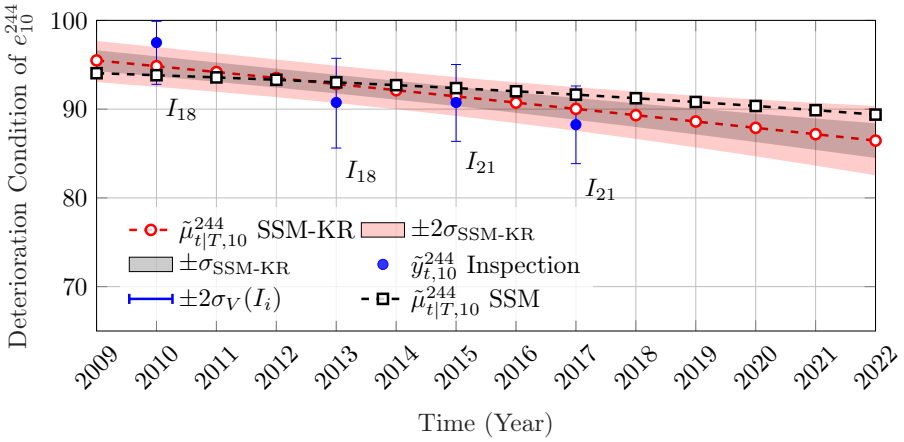

Figure 13: Deterioration condition estimate for real structural element e_{10}^{244} with the *circle* marker representing the SSM-KR estimates and the *square* marker representing SSM estimates.

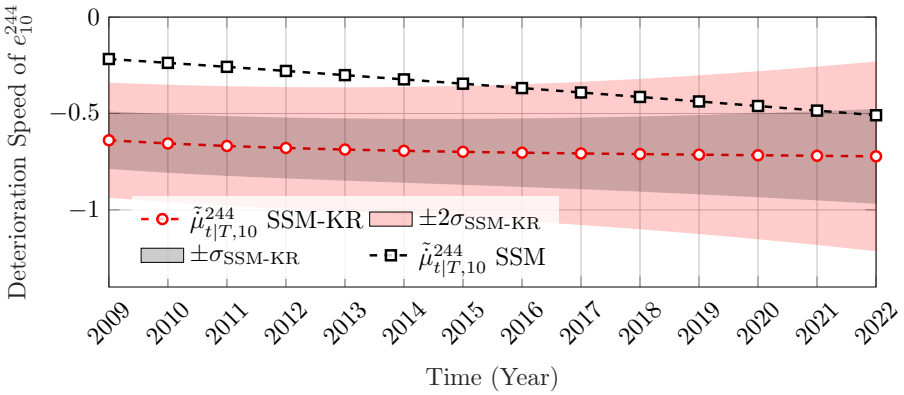

Figure 14: Deterioration speed of structural element e_{10}^{244} with the *circle* marker representing the SSM-KR estimates and the *square* marker representing SSM estimates.

estimates.

The second example is taken from a bridge b_{1599} located at $z_{1599}^3 \approx 46$ with $z_{1599}^2 = 65$ years of age at the time of the first inspection. The structural element e_1^{1599} material is $z_{1599}^1 =$ concrete. The inspection data $\tilde{y}_{t,1}^{1599}$ exhibit a higher variability compared to the first example as shown in Figure 15. Similarly, the SSM-KR estimates show a better adaption to the inspection data in comparison with the SSM model estimates. The deterioration speed estimate associated with e_1^{1599} is shown in Figure 16. The steady estimates of the speed in SSM-KR imply a coherent prior estimate, in comparison to the steep changes in

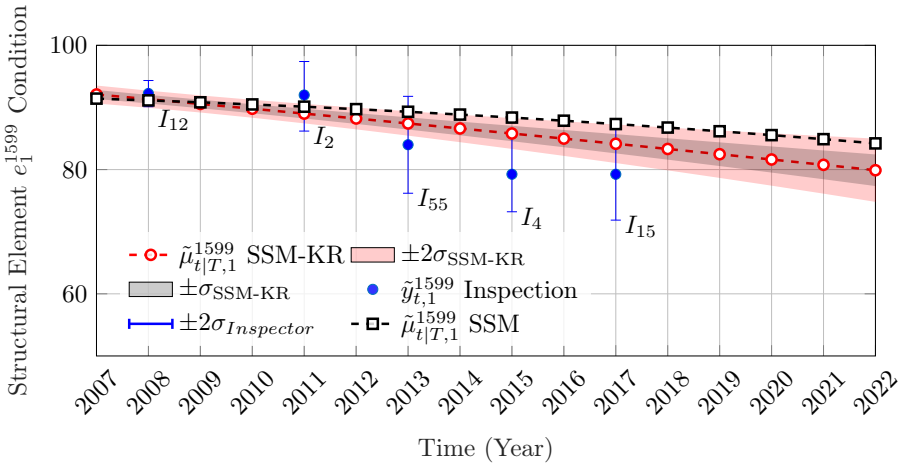

Figure 15: Deterioration condition estimate for real structural element e_1^{1599} with the *circle* marker representing the SSM-KR estimates and the *square* marker representing SSM estimates.

the SSM speed estimates.

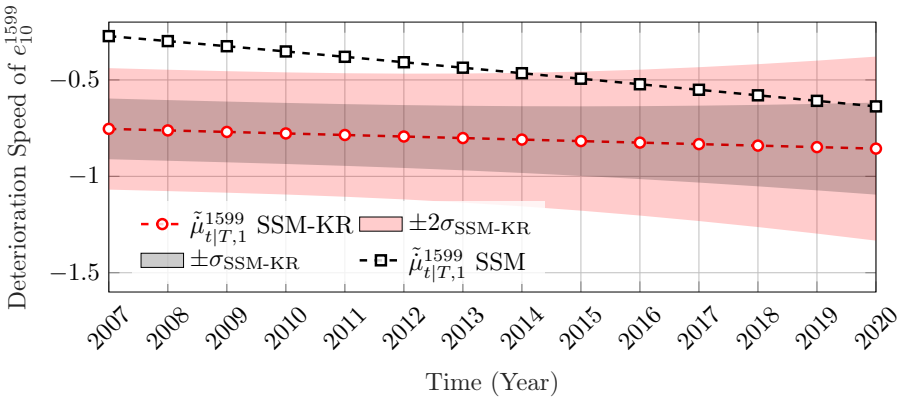

Figure 16: Deterioration speed of structural element e_1^{1599} with the *circle* marker representing the SSM-KR estimates and the *square* marker representing SSM estimates.

The network-scale improvement in the real case is quantified in Table 3, where the log-likelihood associated with the training, the validation and the testing sets are reported. From Table 3, SSM-KR shows a better log-likelihood in each dataset compared to the SSM model.

Table 3: Comparison between SSM-KR and SSM based on the log-likelihood in the training, validation and testing sets

Model	Training	Validation	Testing
SSM	-121175	-17187	-8822
SSM-KR	-116223	-16822	-8482

5 Conclusion

In this study, a hybrid framework based on state-space models and kernel regression is proposed for modeling the deterioration behaviour of bridge-network. The SSM-KR model relies on visual inspection data and takes into account the structural attributes of each bridge. The role of KR is to model patterns between the deterioration speed and the structural attributes. The performance of SSM-KR is verified with synthetic data and benchmarked against a SSM model that does not account for structural attributes. The results have shown that the overall bias in the condition estimates is lower for the SSM-KR, compared to the SSM, as demonstrated by the average error in the forecast time. In addition, the SSM-KR does not show any significant bias toward overestimating or underestimating the initial speed. The analyses also included a validation with real inspections database. Two test cases are considered to demonstrate the model performance. In both cases, the SSM-KR showed a better adaption to the inspection data in comparison with the SSM model. Furthermore, the SSM-KR deterioration speed estimates have a better consistency throughout the analyses time-window. The SSM and SSM-KR are also compared based on the log-likelihood in the training, validation, and testing sets. The SSM-KR has an overall better log-likelihood in each subset of data which emphasizes the importance of factoring structural attributes. Although SSM-KR has a better performance, the model can be computationally demanding. When the number of structural attributes increases $\mathtt{Q} > 5$, the number of reference points required in the KR model becomes large. Nonetheless, overcoming such problem is possible using dimensionality reduction approaches, or by using parametric regression methods. Overall, factoring structural attributes has improved the deterioration model predictive capacity, especially when few inspection points are available, which enables further future analyses such as quantifying the effect of interventions.

Acknowledgements

This project is funded by the Transportation Ministry of Quebec Province (MTQ), Canada. The authors would like to acknowledge the support of René Gagnon for facilitating the access to the inspections database employed in this paper.

References

[1] Duzgun Agdas, Jennifer A Rice, Justin R Martinez, and Ivan R Lasa. Comparison of visual inspection and structural-health monitoring as bridge condition assessment methods. *Journal of Performance of Constructed Facilities*, 30(3):04015049, 2015.

[2] John Aitchison and Colin GG Aitken. Multivariate binary discrimination by the kernel method. *Biometrika*, 63(3):413–420 1976.

[3] Yaakov Bar-Shalom, X Rong Li, and Thiagalingam *Estimation with applications to tracking and navigation: theory algorithms and software*. John Wiley Sons, 2004.

[4] Christopher M *Pattern recognition and machine learning*. springer, 2006.

[5] Miryam Cabieses, Andrew Mikhail, and Namra Khan. Design of a bridge inspection system (bis) to reduce time and cost. 2014.

[6] Leslie E Campbell, Robert J Connor, Julie M Whitehead, and Glenn A Washer. Benchmark for evaluating performance in visual inspection of fatigue cracking in steel bridges. *Journal of Bridge Engineering*, 25(1):04019128

[7] David Duvenaud. Automatic model construction with gaussian processes, 2014.

[8] Cláudia Ferreira, Luís Canhoto Neves, José C Matos, and José Maria Sousa Soares. A degradation and maintenance model: Application to portuguese context. *Proceedings of Bridge Maintenance, Safety, Management and Life Extension*, pages 483–489, 2014.

[9] WR Foster, F Collopy, and LH Ungar. Neural network forecasting of short, noisy time series. *Computers chemical engineering*, 16(4):293–297

[10] Gongkang Fu and Dinesh Devaraj. *Methodology of Homogeneous and Non-homogeneous Markov Chains for Modelling Bridge Element Deterioration*. Michigan Department of Transportation, 2008.

[11] Aurel Galántai. The theory of newton's method. *Journal of Computational and Applied Mathematics*, 124(1-2):25–44

[12] Zachary Hamida and James-A Goulet. State-space models for network-scale analysis of bridge inspection data. In *13th International Conference on Applications of Statistics and Probability in Civil Engineering(ICASP13), Seoul, South Korea*, 2019.

[13] Zachary Hamida and James-A Goulet. Modeling infrastructure degradation from visual inspections using network-scale state-space models. *Structural Control and Health Monitoring*, pages e2582 1545–2255, 2020.

[14] George Hearn. *Framework for a National Database System for Maintenance Actions on Highway Bridges*, volume 668 Transportation Research Board, 2010.

[15] Ying-Hua Huang. Artificial neural network model of bridge deterioration. *Journal of Performance of Constructed Facilities*, 24(6):597–602

[16] Christopher H Jackson. Multi-state models for panel data: the msm package for r. *Journal of statistical software*, 2011.

[17] JD Kalbfleisch and Jerald F Lawless. The analysis of panel data under a markov assumption. *Journal of the American Statistical Association*, 80(392):863–871

[18] MJ Kallen and JM Van Noortwijk. Statistical inference for markov deterioration models of bridge conditions in the netherlands. In *Proceedings of the Third International Conference on Bridge Maintenance, Safety and Management*, number 16-19, 2006.

[19] Rudolf Emil Kalman. Contributions to the theory of optimal control. *Bol. Soc. Mat. Mexicana*, 5(2):102–119, 1960.

[20] Jaeho Lee, Kamalarasa Sanmugarasa, Michael Blumenstein, and Yew-Chaye Loo. Improving the reliability of a bridge management system (bms) using an ann-based backward prediction model (bpm). *Automation in Construction*, 17(6):758–772

[21] Roman Matkovskyy and Taoufik Bouraoui. Application of neural networks to short time series composite indexes: Evidence from the nonlinear autoregressive with exogenous inputs (narx) model. *Journal of Quantitative Economics*, 2018.

[22] *Manuel d'Inspection des Structures*. Ministère des Transports, de la Mobilité Durable et de l'Électrification des Transports, Jan 2014.

[23] Mark Moore, Brent M Phares, Benjamin Graybeal, Dennis Rolander, and Glenn Washer. Reliability of visual inspection for highway bridges, volume i. Technical report, Turner-Fairbank Highway Research Center, 6300 Georgetown Pike, 2001.

[24] Kevin P *Machine learning: a probabilistic perspective*. MIT press, 2012.

[25] Elizbar A Nadaraya. On estimating regression. *Theory of Probability Its Applications*, 9(1): 141–142

[26] See-King Ng and Fred Moses. Bridge deterioration modeling using semi-markov theory. *A. A. Balkema Uitgevers B. V, Structural Safety and Reliability.*, 1:113–120, 1998.

[27] Eugene OBrien, Ciaran Carey, and Jennifer Keenahan. Bridge damage detection using ambient traffic and moving force identification. *Structural Control and Health Monitoring*, 22:1396–1407, 2015.

[28] Goran Puž, Jure Radić, and Irina Stipanovi Oslaković. A new model for stochastic analysis of bridge durability. *Grafëevinar*, 62(04.):287–297 0350–2465, 2010.

[29] Herbert E Rauch, CT Striebel, and F Tung. Maximum likelihood estimates of linear dynamic systems. *AIAA journal*, 3(8):1445–1450 0001–1452, 1965.

[30] Dan Simon and Donald L Simon. Constrained kalman filtering via density function truncation for turbofan engine health estimation. *International Journal of Systems Science*, 41(2):159–171

[31] Jojok Widodo Soetjipto, Tri Joko Wahyu Adi, and Nadjadji Anwar. *Bridge Deterioration Prediction Model Based On Hybrid Markov-System Dynamic*, volume 138. EDP Sciences, 2017.

[32] DM Titterington. A comparative study of kernel-based density estimates for categorical data. *Technometrics*, 22(2):259–268 0040–1706, 1980.

[33] HR Noël Van Erp and André D Orcesi. The use of nested sampling for prediction of infrastructure degradation under uncertainty. *Structure and Infrastructure Engineering*, pages 1–11 1573–2479, 2018.

[34] Christopher KI Williams and Carl Edward Rasmussen. *Gaussian processes for machine learning*, volume 2. MIT press Cambridge, MA, 2006.

[35] Emily K Winn. Artificial neural network models for the prediction of bridge deck condition ratings. Master's thesis, Michigan State University, 2011.

[36] Ivan Zambon, Anja Vidovic, Alfred Strauss, Jose Matos, and Joao Amado. Comparison of stochastic prediction models based on visual inspections of bridge decks. *Journal of Civil Engineering and Management*, 23(5):553–561, 2017. doi: 10.3846/13923730.2017.1323795.

[37] Ivan Zambon, Anja Vidović, Alfred Strauss, and Jose Matos. Condition prediction of existing concrete bridges as a combination of visual inspection and analytical models of deterioration. *Applied Sciences*, 9(1):148, 2019.

[38] Yi Zhang, Chul-Woo Kim, and Kong Fah Tee. Maintenance management of offshore structures using markov process model with random transition probabilities. *Structure and Infrastructure Engineering*, 13(8):1068–1080, 08 2017.

Appendix 1: Pseudo Code

Algorithm 1 Parameter Estimation Framework

Require: $\boldsymbol{\theta}_0^s$: Initial SSM parameters
Require: $\boldsymbol{\theta}_0^\kappa, \dot{\boldsymbol{x}}_{\boldsymbol{z}}$: Initial KR parameters and state respectivly
$L_1 \leftarrow -10^{10}$ (Initial *log-likelihood*), $\epsilon \leftarrow 10^{-3}$ (Convergence tolerance)
$s_1 \leftarrow 1$, $s_2 \leftarrow 1$ (Initial stall),
$\nu_1 \leftarrow 300, \nu_2 \leftarrow 1$ (Iteration limit per parameter)
$\boldsymbol{\theta}_1^s \leftarrow \text{NewtonRaphson}(\mathcal{L}(\boldsymbol{\theta}^s), \boldsymbol{\theta}_0^s, \nu_1)$
$\sigma_V(I_{1:\mathtt{I}}) = \sigma_V,\ \sigma_V \in \boldsymbol{\theta}_1^s$
$L_2 \leftarrow \mathcal{L}(\boldsymbol{\theta}_1^s)$

for $n := 1$ to 5 **do**
  while $|L_{j+1} - L_j| \leq \epsilon$ or $s_1 \geq \rho_1$ **do**
    while $|L_{j+1} - L_j| \leq \epsilon$ or $s_2 \geq \rho_2$ **do**
      $L_j \leftarrow L_{j+1}$
      for $i := 1$ to $\mathtt{I}$ **do**
        if $j = 1$ **then**
          $\sigma_V(I_i) \leftarrow \text{NewtonRaphson}(\mathcal{L}(\sigma_V(I_i)), \boldsymbol{\theta}_j, \nu_2)$
        else $\sigma_V(I_i) \leftarrow \text{NewtonRaphson}(\mathcal{L}(\sigma_V(I_i), \dot{\boldsymbol{x}}_{\boldsymbol{z}}), \boldsymbol{\theta}_j, \nu_2)$
      $L_{j+1} \leftarrow \mathcal{L}(\sigma_V(I_{1:\mathtt{I}}))$
      if $|(L_{j+1} - L_j)/L_j| \leq 0.05$ **then**
        $s_2 = s_2 + 1$
    if $j = 1$ **then**
      $\boldsymbol{\theta}_{j+1}^m \leftarrow \text{NewtonRaphson}(\mathcal{L}(\boldsymbol{\theta}_j^m), \boldsymbol{\theta}_j, \nu_1)$
    else $\boldsymbol{\theta}_{j+1}^m \leftarrow \text{NewtonRaphson}(\mathcal{L}(\boldsymbol{\theta}_j^m, \dot{\boldsymbol{x}}_{\boldsymbol{z}}), \boldsymbol{\theta}_j, \nu_1)$
    $[\boldsymbol{\theta}_{j+1}^\kappa, \dot{\boldsymbol{x}}_{\boldsymbol{z}}] \leftarrow \text{NewtonRaphson}(\mathcal{L}(\boldsymbol{\theta}_j^\kappa, \text{RecursiveEstimation}(\dot{\boldsymbol{x}}_{\boldsymbol{z}})), \boldsymbol{\theta}_j, \nu_1)$
    $L_j \leftarrow \mathcal{L}(\boldsymbol{\theta}_{j+1})$
    $s_1 = s_1 + 1$, $j = j + 1$
return $\boldsymbol{\theta}_{j+1}$ and $\dot{\boldsymbol{x}}_{\boldsymbol{z}}$ (Resulting parameters)

Appendix 2: Kernel Functions

- Aitchison and Aitken kernel function:

$$k^{(\text{AAK})}(z_j, \boldsymbol{z}_c) = \begin{cases} 1 - \ell, & z_j = z_c, \\ \frac{\ell}{\mathtt{C}-1}, & z_j \neq z_c. \end{cases}$$

- Radial basis kernel function:

$$k^{(\mathrm{RBF})}(z_j, \boldsymbol{z}_c) = \exp\left(-\frac{(z_j - \boldsymbol{z}_c)^2}{2\ell^2}\right).$$

- Matérn 12 kernel function:

$$k^{(\mathrm{M12})}(z_j, \boldsymbol{z}_c) = \exp\left(-\frac{(z_j - \boldsymbol{z}_c)}{\ell}\right).$$

- Matérn 52 kernel function:

$$k^{(\mathrm{M52})}(z_j, \boldsymbol{z}_c) = \left(1 + \frac{\sqrt{5}(z_j - \boldsymbol{z}_c)}{\ell} + \frac{5}{3}\frac{(z_j - \boldsymbol{z}_c)^2}{\ell^2}\right)\exp\left(-\frac{\sqrt{5}(z_j - \boldsymbol{z}_c)}{\ell}\right).$$